Acta Crystallographica Section D
Biological Crystallography
ISSN 0907-4449

Structure of an ETHE1-like protein from *Arabidopsis thaliana*

Jason G. McCoy,[a] Craig A. Bingman,[a] Eduard Bitto,[a] Meghan M. Holdorf,[b] Christopher A. Makaroff[b] and George N. Phillips Jr[a]*

[a]Department of Biochemistry and Center for Eukaryotic Structural Genomics, University of Wisconsin–Madison, USA, and [b]Department of Chemistry and Biochemistry, Miami University, USA

Correspondence e-mail: phillips@biochem.wisc.edu

Received 12 April 2006
Accepted 31 May 2006

PDB Reference: AtETHE1, 2gcu, r2gcusf.

The protein product of gene At1g53580 from *Arabidopsis thaliana* possesses 54% sequence identity to a human enzyme that has been implicated in the rare disorder ethylmalonic encephalopathy. The structure of the At1g53580 protein has been solved to a nominal resolution of 1.48 Å. This structure reveals tertiary structure differences between the ETHE1-like enzyme and glyoxalase II enzymes that are likely to account for differences in reaction chemistry and multimeric state between the two types of enzymes. In addition, the *Arabidopsis* ETHE1 protein is used as a model to explain the significance of several mutations in the human enzyme that have been observed in patients with ethylmalonic encephalopathy.

1. Introduction

The *Arabidopsis thaliana* gene At1g53580 encodes a 255-residue protein whose sequence places it in the metallo-β-lactamase superfamily (SUPFAM E value = 3×10^{-13}; Gough *et al.*, 2001). This protein was originally identified as one of five glyoxalase II isozymes in *Arabidopsis* (Maiti *et al.*, 1997). Structures of two glyoxalase II enzymes are currently known. One corresponds to a cytoplasmic isozyme from *Homo sapiens* (Cameron *et al.*, 1999) and the other is a mitochondrial isozyme from *A. thaliana* (Marasinghe *et al.*, 2005), which has been designated AtGLX2-5 (At2g31350).

Glyoxalase II (GLX2; also known as hydroxyacylglutathione hydrolase) along with glyoxalase I (GLX1) makes up the glyoxalase system that acts to convert a variety of α-keto aldehydes into hydroxyacids in the presence of glutathione (Thornalley, 1993). Aromatic and aliphatic α-keto aldehydes react spontaneously with glutathione to form thiohemiacetals, which are converted to *S*-(2-hydroxyacyl)-glutathione derivatives by GLX1. GLX2 hydrolyzes these derivatives to regenerate glutathione and produce hydroxyacids. Glyoxalase I utilizes a number of α-ketoaldehydes (Davidson *et al.*, 2000). However, the primary physiological substrate of the enzyme is thought to be methylglyoxal (MG), a cytotoxic and mutagenic compound formed primarily as a byproduct of carbohydrate and lipid metabolism (Thornalley, 1995, 1998). Therefore, the glyoxalase system is thought to play an important role in chemical detoxification. Glyoxalase II enzymes, like other members of the metallo-β-lactamase superfamily, have been shown to contain dinuclear metal centers (Crowder *et al.*, 1997). Interestingly, different glyoxalase II enzymes have differing specificities for iron, zinc and manganese (Wenzel *et al.*, 2004; Crowder *et al.*, 1997; Marasinghe *et al.*, 2005; Cameron *et al.*, 1999).

Recently, it has been shown that the predicted At1g53580 enzyme shows greater sequence identity (54%) to a human enzyme from a gene named ETHE1 than to glyoxalase II enzymes. Therefore, the *Arabidopsis* gene locus At1g53580 has been named AtETHE1. We will subsequently refer to the protein product of this gene as AtETHE1 as well. While the ETHE1 protein (referred to hereafter as ETHE1) shows significant sequence similarity to glyoxalase II, it does not possess glyoxalase II activity (Tiranti *et al.*, 2004). No function has been determined for the enzyme; however, it has been implicated in a rare autosomal recessive disorder known as ethylmalonic encephalopathy and a number of mutations in the ETHE1 protein of affected individuals have been identified (Tiranti *et al.*, 2004). The first description of this disorder included the following symptoms: mental retardation, orthostatic acrocyanosis, relapsing petechiae, progressive pyramidal signs, chronic diarrhea and symmetric brain lesions (Burlina *et al.*, 1991, 1994). There were also high levels of ethylmalonic acid, C4–C5 acylglycines and acylcarnitines detected in patients' urine as well as elevated levels of lactic acid and short- and branched-chain acylcarnitine levels in the blood (Burlina *et al.*, 1991, 1994).

In this paper, we describe the structure of AtETHE1 and demonstrate the structural differences between AtETHE1 and glyoxalase II enzymes. We further illustrate the structural significance of several mutations within the ETHE1 enzyme found in sufferers of ethylmalonic encephalopathy.

2. Materials and methods

2.1. Cloning, expression and purification

The AtETHE1 cDNA was cloned into pET24b as an *Nde*I and *Xho*I fragment following PCR amplification using the primers 3′-TCTTCTCATATGAAGCTTCTCTTTCGTCAAC and 5′-GAGTCGACTCGAGCTCTAGATC$(T)_{16}$. For high-level expression in *Escherichia coli*, the N-terminal 11 amino acids were removed and the amino-terminal methionine placed at amino acid 12 of the predicted protein sequence. After verification by DNA sequencing, pET24b-AtETHE1 was transformed into BL21-Codon Plus (DE3)-RIL cells and used for protein overexpression in ZY medium containing 50 µg ml^{-1} kanamycin and 50 µ*M* $Fe(NH_4)_2(SO_4)_2$ as described previously (Zang *et al.*, 2001). AtETHE1 was purified from cleared lysates by FPLC using a Q-Sepharose column as described previously (Crowder *et al.*, 1997). Protein purity was determined by SDS–PAGE and protein concentrations were determined using the extinction coefficient 10 240 M^{-1} cm^{-1}, which is based on the amino-acid composition of AtETHE1 (Gill & von Hippel, 1989). Metal analyses were performed on the purified enzyme using a Varian Liberty 150 inductively coupled plasma spectrometer with atomic emission spectroscopy detection (ICP–AES) as described by Crowder *et al.* (1997).

2.2. Crystallization

AtETHE1 crystals were grown by the hanging-drop vapor-diffusion method at 293 K. The reservoir solution contained 24%(*w*/*v*) polyethylene glycol methyl ether 5K, 0.05 *M* magnesium sulfate and 0.10 *M* *N*-(2-hydroxyethyl)piperazine-*N*′-(2-ethanesulfonic acid) (HEPES) pH 8.5. The protein solution contained 10 mg ml^{-1} protein and 10 m*M* MOPS pH 7.2. Drops were produced by mixing 2 µl protein solution with 2 µl reservoir solution on a Nextal cover slip (Nextal

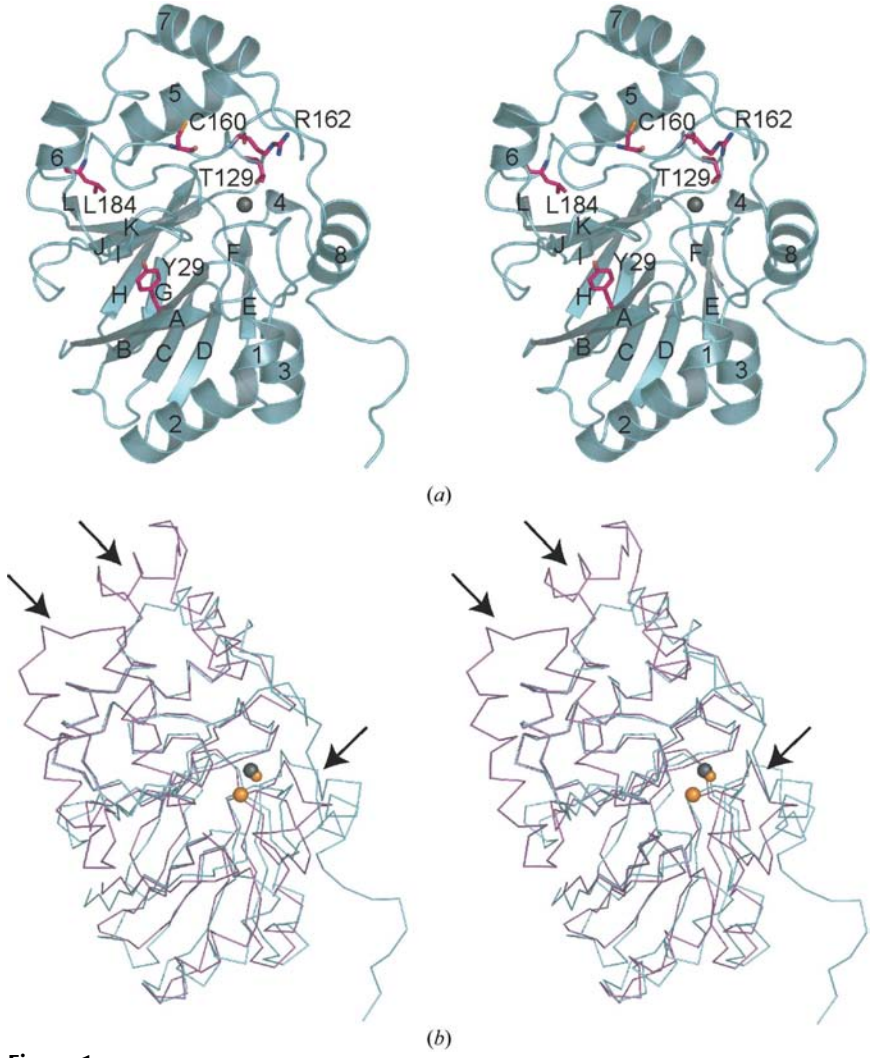

Figure 1
(*a*) The At1g53580 monomer. Helices are labelled 1–8 and β-strands are labelled *A*–*L*. Residues known to be involved in human ethylmalonic encephalopathy in human ETHE1 are colored pink. (*b*) Overlay of the AtETHE1 (cyan) and the GLX2-5 (magenta) monomers. The metal ions from the GLX2-5 structure are colored orange and the iron ion from the AtETHE1 structure is colored gray. Arrows point to changes between the folds of the two enzymes.

Table 1
Summary of crystallographic data-collection and refinement statistics.

Values in parentheses refer to the highest resolution shell.

Data set	Native	Hg derivative
Data collection		
Wavelength (Å)	1.23984	0.98244
Resolution range (Å)	46.11–1.48 (1.51–1.48)	49.11–2.04 (2.09–2.04)
Space group	$P2_1$	$P2_1$
Unit-cell parameters		
a (Å)	66.6	
b (Å)	64.5	
c (Å)	127.9	
β (°)	97.8	
Measured/unique reflections	1005815/170395	448871/66747
Completeness (%)	94.6 (67.7)	97.0 (73.9)
$R_{\rm merge}$	0.075 (0.435)	0.128 (0.364)
Average $I/\sigma(I)$	12.43 (2.82)	8.07 (2.29)
Redundancy	5.9 (2.5)	6.7 (3.5)
Phasing		
Mean FOM (centric/acentric)		0.29966/0.31622
Isomorphous $R_{\rm cullis}$ (centric/acentric)		0.851/0.850
Anomalous $R_{\rm cullis}$		0.919
Refinement statistics		
$R_{\rm cryst}/R_{\rm free}$ (%)	17.7/20.4	
Ramachandran plot		
Most favorable regions (%)	92.0	
Additionally allowed regions (%)	8.0	
Generously allowed regions (%)	0.0	
Disallowed regions (%)	0.0	
R.m.s. deviations from ideality		
Bonds (Å)	0.015	
Angles (°)	1.636	
Average B value (Å^2)	19.4	
Average protein B value (Å^2)	17.5	
Average solvent B value (Å^2)	32.5	

Biotechnologies, Montreal). Two to three drops were placed on each cover slip and the cover slip was then used to seal a tray well containing 500 µl reservoir solution. The crystals were grown at room temperature and diffraction-quality crystals appeared after several months. Additional crystals used for phasing were grown within a week following micro-seeding and then soaked in a solution of mother liquor containing 2 mM thimerosal ($C_9H_9HgNaO_2S$) for 2 days. Crystals were then cryoprotected by soaking in solutions of mother liquor with increasing amounts of ethylene glycol up to 20%(v/v).

2.3. Data collection

Diffraction data from the native AtETHE1 crystal were collected at liquid-nitrogen temperatures on beamline 22-ID at Argonne National Laboratories at a wavelength of 1.23984 Å to a maximum resolution of 1.48 Å. Data were collected on a MAR 300 charge-coupled device using 2 s exposures and a frame width of 1°. Diffraction data from the mercury-derivatized crystal were collected on beamline 23ID-B at Argonne National Laboratories at a wavelength of 0.98244 Å to a maximum resolution of 2.04 Å. Data were collected on a MAR 300 charge-coupled device using 6 s exposures and a frame width of 1°. The diffraction images were integrated and scaled using *HKL*-2000 (Otwinowski & Minor, 1997). The overall anomalous R factor for the derivative data set as calculated by *SCALEPACK* was 0.062 and the overall R factor between the native and derivative data set was 0.224.

2.4. Structure determination and refinement

The mercury substructure of the derivatized crystal was determined using *HySS* from *PHENIX* (Adams *et al.*, 2002; Weeks *et al.*, 2003), which detected four Hg atoms within the asymmetric unit. The mercury positions were input into *autoSHARP* to calculate phases using single isomorphous replacement with anomalous scattering phasing techniques (Bricogne *et al.*, 2003). Auxiliary programs used by *autoSHARP* were from the *CCP*4 suite (Collaborative Computational Project, Number 4, 1994). Density modification was carried out with *SOLOMON* (Abrahams & Leslie, 1996). *ARP*/*wARP* was used to build the initial model (Lamzin & Wilson, 1993). The model was completed with alternate rounds of model building with *Coot* (Emsley & Cowtan, 2004) and restrained refinement *via REFMAC* (Murshudov *et al.*, 1997).

The final model contained four protein molecules, four iron(II) ions, 1037 water molecules, 14 ethylene glycol molecules and a sulfate molecule. Eight of the C-terminal residues for two of the protein chains and the final C-terminal residue for the other two chains were left unmodeled. The discrepancy in the observable length of the four chains arose from additional non-biological contacts that the C-terminal regions of chains A and C were able to make with chains D and B. The Ramachandran plot showed that 92% of the residues were in the most favorable region. The remainder were in the generously allowed region of the plot. The data-collection and refinement statistics are summarized in Table 1.

3. Results and discussion

3.1. Overall fold

The overall fold of AtETHE1 is typical of the β-lactamase superfamily. It contains two central mixed β-sheets, each containing six strands, surrounded on both sides by helices (see Fig. 1). The β-sheet topology is of the order A, B, C, D, E, F and G, H, I, J, K, L. β-Strands A, B and C are aligned antiparallel, whereas C, D, E and F are parallel. In the second β-sheet, strands G, H, I and J are aligned antiparallel, J and K are aligned parallel and K and L are aligned antiparallel.

A *VAST* search indicated that the most structurally similar enzymes are the human and *Arabidopsis* (AtGLX2-5) glyoxalase II enzymes, with scores of 27.7 and 27.2, respectively. The overall folds of AtETHE1 and AtGLX2-5 are highly similar, but differ in three regions, as shown in Fig. 1. The first two regions are outside the active site but make contacts with one another. This includes a two-helix bundle that extends from residues 172 to 206 and an extended loop consisting of residues 223–240 in AtGLX2-5. Both of these features are missing in AtETHE1. Additionally, the extended C-terminus of AtETHE1 reaches across the opening of the active site,

greatly limiting the possible size of potential substrates. These gaps are further illustrated in Fig. 2.

3.2. Dimer

While previously described glyoxalase II enzymes are monomers, the crystal structure of AtETHE1 reveals a dimeric organization for the protein (see Fig. 3). The human ETHE1 protein was shown to be a dimer by gel-filtration chromatography. Interestingly, the dimerization interface for AtETHE1 appears to be in a region that was blocked by the two-helix bundle of the AtGLX2-5 enzyme. This may represent a distinguishing feature between ETHE1-like and glyoxalase II enzymes. The interface between the AtETHE1 dimers is not extensive, with only 830 Å^2 of buried surface area (Jones & Thornton, 1995). The interface contains 58% nonpolar area and involves ten residue-to-residue hydrogen bonds. The interactions are identical in the two subunits, with Arg17 forming hydrogen bonds with Glu206 from the other subunit and likewise Gln18 with Glu200, Phe20 with Gly198, Arg53 with Lys197, Glu60 with Arg158 and *vice versa*.

3.3. Metal-binding site

Only one metal atom was located within the electron density for AtETHE1. ICP–AES results indicated that the purified enzyme contained two molar equivalents of iron; however, ICP–MS metal analysis of the protein after being subjected to freezing and storage gave a metal/protein ratio of 0.56. This closely matches what was observed in the crystal structure, where an occupancy of 0.5 for the iron ion gave the best refinement results. Despite this partial occupancy, the electron density for the coordinating ligands is well defined without any indication of heterogeneity or multiple conformers.

The iron ion location is identical to one of the two metal ions in the AtGLX2-5 protein structure. Fig. 4 depicts an overlay of the residues involved in metal binding in the AtGLX2-5 and AtETHE1 enzymes. In the AtGLX2-5 protein structure, one metal ion was tetrahedrally coordinated to three histidines (His54, His56 and His112) and a bridging water molecule. The coordination of the equivalent iron ion in the AtETHE1 structure was octahedral. In addition to three waters, the iron ion was bound to His72 and His128, the homologs of His54 and His112 in AtGLX2-5. The homolog of Asp131, Asp153, which binds the second metal atom in AtGLX2-5, is slightly shifted such that it also directly coordinates the iron ion in AtETHE1. The homolog of His56, His74, does not coordinate the metal in AtETHE1.

In the AtGLX2-5 structure there is a single-turn helix containing His56 near its N-terminal end. In the AtETHE1 structure, this helix has been pulled apart such that the side chain of His74 is no longer directed towards the metal atom. This change also displaces the side chains of Asp76 and His77, whose structural equivalents in AtGLX2-5 coordinate the second metal. It is unclear if the unwinding of this helix simply arises from a missing metal atom or if it accurately represents an active conformation of the protein. There are two sequence features of AtETHE1 that indicate this unraveling may be more likely to occur in this enzyme than in the glyoxylase II isozymes. The unwinding of this helix places the side chain of Ala75 directly into the active site of the enzyme. In glyoxylase II enzymes, this alanine is replaced by a residue with a bulky side chain, for instance a tyrosine in AtGLX2-5, which may cause additional steric problems upon unwinding of the helix. In addition, there is a modification to a conserved glyoxylase II CGK(L/F)(F/Y)EG motif (Cys138, Gly139, Lys140, Leu141, Phe142, Glu143 and Gly144 in AtETHE1) which alters the sequence to CGRTDFQEG. The side chain of the inserted glutamine, Gln166, directly occupies the space where the side chain of His74 would need to be to coordinate the Fe ion and forms a hydrogen bond with the carbonyl of Val73. This displacement is further stabilized by hydrogen bonds formed between the side chains of Asp164 and Arg162. These residues appear to be strongly conserved in ETHE1 proteins.

The second metal atom in AtGLX2-5 was coordinated by His59, His169, Asp58, Asp131 and a bridging water molecule. As mentioned previously, the homologs of His59 and Asp58 in AtETHE1 are displaced owing to the unraveling of a single-turn helix; however, the homolog of Asp58 (Asp76) is still within coordination distance of a second metal atom. The homolog of His59 (His77) is pulled away from the putative second metal atom site and in its current position is unlikely to coordinate a metal atom. The side chain of His74 in the AtETHE1 enzyme is near the location His77 would need to occupy if it were to coordinate a second metal atom and may serve as a replacement for binding a second metal atom. In the AtETHE1 structure a carboxyl O atom of the homolog of Asp131 is 2.1 Å from the iron ion and also near the expected location of the second metal atom. The homolog of His169, His194, is positioned identically to His169 and could conceivably coordinate a second metal atom in AtETHE1. Ultimately, all of the residues necessary for binding a second metal atom similarly to GLX2-5 are present in AtETHE1; however, some structural rearrangements would have to occur to obtain the necessary orientation of the metal-binding side chains.

The metal and potential substrate-binding residues in AtETHE1 are for the most part involved in the same hydrogen-bonding networks observed in AtGLX2-5. The primary exception is His194, which does not coordinate a metal in the AtETHE1 structure. The equivalent histidine in AtGLX2-5 was stabilized by interactions with the carboxyl O atom of an aspartate side chain. The remaining carboxyl O atom was hydrogen bonded to a lysine side-chain N atom. In AtETHE1, this aspartate is replaced with a serine, limiting further electron delocalization. Also, the imidazole side chain of His194 is flipped in the AtETHE1 structure and the ND1 N atom instead interacts with the side chain of Asp153.

3.4. Active site

Residues involved in substrate binding in the human glyoxalase II are almost entirely conserved in AtGLX2-5. This is not the case with AtETHE1. An overlay of the human

```
                                                   *
AtETHE1    MGSS----------SSFSSSSKLLFRQLFENESSTFTYLLADVSHPDKPALLIDPVDKTVDRDLKLID 59
ETHE1      MAEAVLRVARRQLSQRGGSGAPILLRQMFEPVSCTFTYLLGDRES--REAVLIDPVLETAPRDAQLIK 66
AtGLX2-5   ----------------------MQIELVPCLK-DNYAYILHDEDT--GTVGVVDPS--EAEPIIDSLK 41
HumanGLX2  ----------------------MKVEVLPALT-DNYMYLVIDDET--KEAAIVDPV--QPQKVVDAAR 41

AtETHE1    ELGLKLIYAMNTHVHADHVTGTGLLKTKLPGVKSVISKASGSK---ADLFLEPGDKVSIGDIYLEVRA 124
ETHE1      ELGLRLLYAVNTHCHADHITGSGLLRSLLPGCQSVISRLSGAQ---ADLHIEDGDSIRFGRFALETRA 131
AtGLX2-5   RSGRNLTYILNTHHHYDHTGGNLELKDRY-GAKVIGSAMDKDRIPGIDMALKDGDKWMFAGHEVHVMD 108
HumanGLX2  KHGVKLTTVLTTHHHWDHAGGNEKLVKLESGLKVYG---GDDRIGALTHKITHLSTLQVGSLNVKCLA 106

               *                              * *                      *
AtETHE1    TPGHTAGCVTYVTGEGADQPQPRMAFTGDAVLIRGCGRTDFQEGGSSDQLYESVHSQIFTLPKDTLIY 191
ETHE1      SPGHTPGCVTFVLNDHS------MAFTGDALLIRGCGRTDFQQGGCAKTLYHSVHEKIFTLPGDCLIY 192
AtGLX2-5   TPGHTKGHISLYFPGS------RAIFTGDTMFSLSCGKL--FEGGTPKQMLASLQ-KITSLPDDTSIY 166
HumanGLX2  TPCHTSGHICYFVSKPG-GSEPPAVFTGDTLFVAGCGKF--YEGGTADEMCKALLEVLGRLPPDTRVY 170

AtETHE1    PAHDYK--------------------------------GFEVITVGEEMQHNPRLTK----------- 216
ETHE1      PAHDYH--------------------------------GFTVSTVEEERTLNPRLTL----------- 217
AtGLX2-5   CGHEYTLSNSKFALSLEPNNEVLQSYAAHVAELRSKKLPTIPTTVKMEKACNPFLRS---------SN 225
HumanGLX2  CGHEYTINNLKFARHVEPGNAAIREKLAWAKEKYSIGEPTVPSTLAEEFTYNPFMRVREKTVQQHAGE 238

AtETHE1    --------------DKETFKTIMSNLNLSYPKMIDVAVPANMVCGLQDVPSQAN 256
ETHE1      --------------SCEEFVKIMGNLNLPKPQQIDFAVPANMRCGVQTPTA--- 254
AtGLX2-5   TDIRRALRIPEAADEAEALGIIRKAKDDF------------------------- 254
HumanGLX2  TDPVTTMRAVRREKDQFKMPRD-------------------------------- 260
```

Figure 2
Sequence alignment of AtETHE1, human ETHE1, AtGLX2-5 and human glyoxalase II (HumanGLX2). The alignment was created by running a structure-based alignment with *VAST* between AtETHE1 and GLX2-5 and then performing a pairwise alignment between AtETHE1 and human ETHE1 and between GLX2-5 and human glyoxalase II. Residues involved in dimer formation in AtETHE1 are colored green, residues involved in substrate binding in human glyoxalase II are colored orange, residues which belong to metal site 1 are colored blue, residues which belong to metal site 2 are colored red and residues that have been implicated in ethylmalonic encephalopathy are marked with an asterisk.

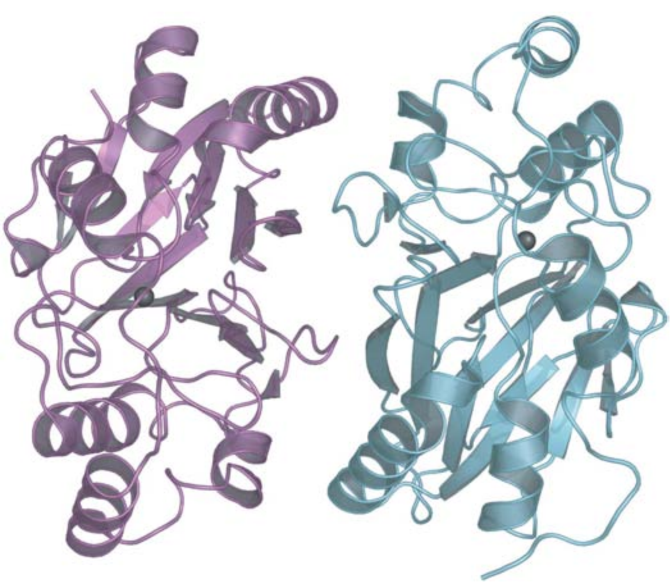

Figure 3
The AtETHE1 dimer. The two subunits are colored cyan and magenta.

glyoxalase II substrate-binding site with the equivalent residues in AtETHE1 is depicted in Fig. 5. The side chains of residues Arg249 and Lys252 make hydrogen bonds with the glycine portion of glutathione in the human enzyme. These residues are replaced with Met225 and Leu228 in AtETHE1. Leu228 is also pulled away from the substrate-binding region. The backbone amino group of Lys143 and the side chain of Tyr175 in human glyoxalase II were shown to hydrogen bond to the cysteine portion of glutathione. In AtETHE1, Lys143 is replaced by Arg162; however, the backbone amino groups of these two residues overlap. Replacement of this lysine with arginine appears to be common among ETHE1 proteins and loss of this arginine has been linked with ethylmalonic encephalopathy in humans (Tiranti *et al.*, 2006). The AtETHE1 homolog of Tyr175, Tyr196, is also positioned similarly to that of the human enzyme. In human glyoxalase II the side chains of Tyr145 and Lys143 form hydrogen bonds with the glutamate portion of the glutathione. AtETHE1 has a phenylalanine in place of Tyr145; however, *Arabidopsis* glyoxalase II AtGLX2-5 has the same substitution. Lys143 is replaced by Arg162 in AtETHE1. The arginine side chain could conceivably also interact with the substrate. The side chain of Arg162 appears to be firmly held in place by two hydrogen bonds with the side-chain carboxyl of Asp164 and is not likely to be as flexible as Lys143.

The active site of AtETHE1 has significantly less room for substrate binding than that of the human and *Arabidopsis* glyoxalase II enzymes owing to the unwound helix described above and the extended C-terminal region that covers up much of the active site. While there appears to be enough room to fit a glutathione group, there is substantially less space available for the other portion of the thioester. The other subunit of the dimer does not appear to alter the active site.

3.5. Structural basis for encephalopathy

A number of single-residue mutations have been identified in the ETHE1 protein of patients with ethylmalonic encephalopathy (Tiranti *et al.*, 2004, 2006) and a model of human ETHE1 was created based on the human glyoxalase II crystal structure (Tiranti *et al.*, 2006). Our results confirm many of the observations of this study and provide some additional details (Fig. 1). Mutations in human ETHE1 include R163Q, C161Y, Y38C, L185R and T136A. The *Arabidopsis* equivalent of Arg163, Arg162, is located within the expected active site of the enzyme and forms two hydrogen bonds with the side chain of Asp164. Given the location of Arg162, it seems likely that this residue may be directly involved in the catalytic mechanism of the enzyme. The *Arabidopsis* equivalent of Cys161, Cys160, is also near the active site. Mutation of this residue into a bulky tyrosine would clearly reposition Arg162 and possibly other amino acids involved in substrate binding. The *Arabidopsis* equivalent of Thr136, Thr129, forms a hydrogen bond with a backbone amine N atom that may help stabilize His128, which coordinates the iron ion in AtETHE1. The *Arabidopsis* equivalent of Tyr38, Tyr29, is part of the hydrophobic interface between the two internal β-sheets and

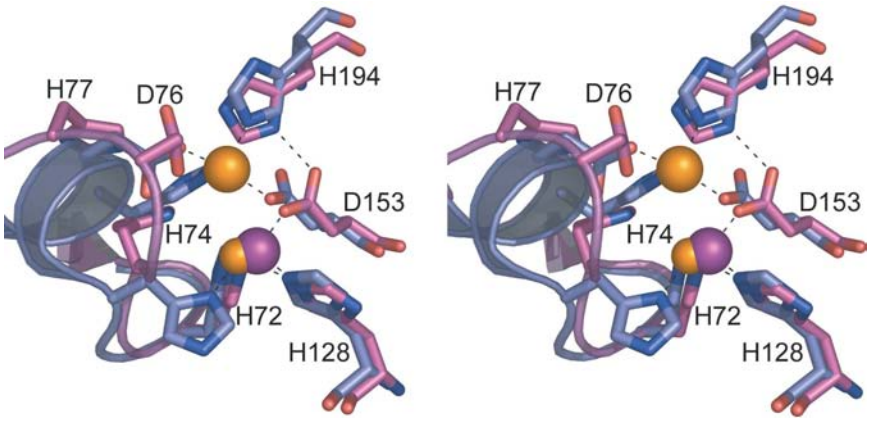

Figure 4
Overlay of metal-binding residues in the AtETHE1 enzyme (magenta) and the GLX2-5 enzyme (cyan). The metal ion from the AtETHE1 structure is colored purple. The metal ions from the GLX2-5 structure are colored orange. The backbone of both enzymes is also depicted in order to illustrate the unwinding of the helix near the metal-binding site. Labels correspond to AtETHE1.

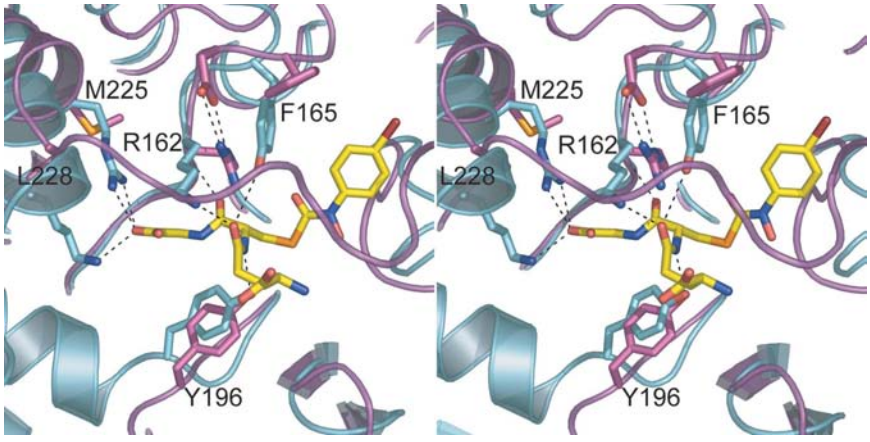

Figure 5
Overlay of the substrate-binding residues from the human glyoxalase II (cyan) with the equivalent residues in the AtETHE1 enzyme (magenta). *S*-Hydroxybromophenylcarbamoyl glutathione bound to glyoxalase II is colored yellow. Labels correspond to AtETHE1.

sits in a pocket of cyclic aromatic side chains which include Phe27, Phe16, Phe156 and Tyr191. In addition, the Tyr29 hydroxyl group forms a hydrogen bond with the side chain of Gln18, which is part of the dimer interface. Mutation of this residue could subsequently have repercussions on the stability of both the tertiary and quaternary structures. The *Arabidopsis* equivalent of the final relevant human residue, Leu184, is far from the active site and sits in the region between the C-terminal β-sheet and the C-terminal α-helical region. The residue is near the side chains of Arg123 and Arg147. Mutation of this residue to another arginine would be likely to be highly destabilizing.

3.6. Sequence analysis

A series of *BLAST* searches were conducted to determine the prevalence of ETHE1-like enzymes. The assumption was made that the presence of Arg162, the absence of residues involved in binding glutathione and the absence of the two-helix bundle observed in glyoxalase II are features that distinguish between ETHE1 and glyoxalase II enzymes. ETHE1-like enzymes have been observed in almost all forms of life, including animals, plants, fungi, eubacteria and archaebacteria. Unlike glyoxalase II enzymes, multiple isozymes of the ETHE1 have not been detected within a species. It was also noted that in some archaebacteria, such as halobacteria, the ETHE1-like fold was coupled to a rhodanese transferase-like domain.

4. Conclusions

The crystal structure of AtETHE1 has been solved and refined to 1.48 Å. The structure reveals a fold that varies from the closely related enzyme glyoxalase II. The removal of a two-helix bundle in AtETHE1 results in the formation of a dimer interface that is missing from the glyoxalase II enzymes. The extended C-terminus which aligns the active site, as well as several changes in the substrate-binding residues of glyoxalase II enzymes, allow a different and unknown reaction chemistry. The structure also revealed a metal-binding site as well as a possible second metal site given some structural rearrangement. In addition, the structure of AtETHE1 is the closest model available for human ETHE1 and provides a structural explanation for the deleterious effects of several mutations corresponding to the onset of ethylmalonic encephalopathy as well as revealing the active-site architecture involved in binding an as yet unknown substrate.

This work was supported by the National Institutes of Health, Protein Structure Initiative P50 GM 64598, U54 GM 074901 (John L. Markley, PI; GNP and Brian G. Fox, Co-Investigators), NLM training grant T15 LM007359 (JGM) and the National Science Foundation MCB-9817083 (CAM). The Advanced Photon Source is supported by the US Department of Energy, Basic Energy Sciences, Office of Science under contract No. W-31-109-ENG-38. Data were collected at Southeast Regional Collaborative Access Team (SER-CAT) 22-ID beamline at the Advanced Photon Source, Argonne National Laboratory. Supporting institutions may be found at http://www.ser-cat.org/members.html. GM/CA CAT is supported by the National Cancer Institute (Y1-CO-1020) and the National Institute of General Medical Science (Y1-GM-

1104). We thank Ward Smith for assistance at GM/CA-CAT. We specially thank Gary Wesenberg, Dave Aceti, Janelle Warick and other members of the CESG staff.

References

Abrahams, J. P. & Leslie, A. G. W. (1996). *Acta Cryst.* D**52**, 30–42.

Adams, P. D., Grosse-Kunstleve, R. W., Hung, L. W., Ioerger, T. R., McCoy, A. J., Moriarty, N. W., Read, R. J., Sacchettini, J. C., Sauter, N. K. & Terwilliger, T. C. (2002). *Acta Cryst.* D**58**, 1948–1954.

Bricogne, G., Vonrhein, C., Flensburg, C., Schiltz, M. & Paciorek, W. (2003). *Acta Cryst.* D**59**, 2023–2030.

Burlina, A., Dionisi-Vici, C., Bennett, M. J., Gibson, K. M., Servidei, S., Bertini, E., Hale, D. E., Schmidt-Sommerfeld, E., Sabetta, G., Zacchello, F. & Rinaldo, P. (1994). *J. Pediatr.* **124**, 79–86.

Burlina, A., Zacchello, F., Dionisi-Vici, C., Bertini, E., Sabetta, G., Bennett, M. J., Hale, D. E., Schmidt-Sommerfeld, E. & Rinaldo, P. (1991). *Lancet*, **338**, 1522–1523.

Cameron, A. D., Ridderstrom, M., Olin, B. & Mannervik, B. (1999). *Structure*, **7**, 1067–1078.

Collaborative Computational Project, Number 4 (1994). *Acta Cryst.* D**50**, 760–763.

Crowder, M. W., Maiti, M. K., Banovic, L. & Makaroff, C. A. (1997). *FEBS Lett.* **418**, 351–354.

Davidson, G., Clugston, S. L., Honek, J. F. & Maroney, M. J. (2000). *Inorg. Chem.* **39**, 2962–2963.

Emsley, P. & Cowtan, K. (2004). *Acta Cryst.* D**60**, 2126–2132.

Gill, S. C. & von Hippel, P. H. (1989). *Anal. Biochem.* **182**, 319–326.

Gough, J., Karplus, K., Hughey, R. & Chothia, C. (2001). *J. Mol. Biol.* **313**, 903–919.

Jones, S. & Thornton, J. M. (1995). *Prog. Biophys. Mol. Biol.* **63**, 31–65.

Lamzin, V. S. & Wilson, K. S. (1993). *Acta Cryst.* D**49**, 129–147.

Maiti, M. K., Krishnasamy, S., Owen, H. A. & Makaroff, C. A. (1997). *Plant Mol. Biol.* **35**, 471–481.

Marasinghe, G. P., Sander, I. M., Bennett, B., Periyannan, G., Yang, K. W., Makaroff, C. A. & Crowder, M. W. (2005). *J. Biol. Chem.* **280**, 40668–40675.

Murshudov, G. N., Vagin, A. A. & Dodson, E. J. (1997). *Acta Cryst.* D**53**, 240–255.

Otwinowski, Z. & Minor, W. (1997). *Methods Enzymol.* **276**, 307–326.

Thornalley, P. J. (1993). *Mol. Aspects Med.* **14**, 287–371.

Thornalley, P. J. (1995). *Crit. Rev. Oncol. Hematol.* **20**, 99–128.

Thornalley, P. J. (1998). *Chem. Biol. Interact.* **111–112**, 137–151.

Tiranti, V., Briem, E., Lamantea, E., Mineri, R., Papaleo, E., Degioia, L., Forlani, F., Rinaldo, P., Dickson, P., Abu-Libdeh, B., Cindro-Heberle, L., Owaidha, M., Jack, R. M., Christensen, E., Burlina, A. & Zeviani, M. (2006). *J. Med. Genet.* **43**, 340–346.

Tiranti, V., D'Adamo, P., Briem, E., Ferrari, G., Mineri, R., Lamantea, E., Mandel, H., Balestri, P., Garcia-Silva, M. T., Vollmer, B., Rinaldo, P., Hahn, S. H., Leonard, J., Rahman, S., Dionisi-Vici, C., Garavaglia, B., Gasparini, P. & Zeviani, M. (2004). *Am. J. Hum. Genet.* **74**, 239–252.

Weeks, C. M., Adams, P. D., Berendzen, J., Brunger, A. T., Dodson, E. J., Grosse-Kunstleve, R. W., Schneider, T. R., Sheldrick, G. M., Terwilliger, T. C., Turkenburg, M. G. & Usón, I. (2003). *Methods Enzymol.* **374**, 37–83.

Wenzel, N. F., Carenbauer, A. L., Pfiester, M. P., Schilling, O., Meyer-Klaucke, W., Makaroff, C. A. & Crowder, M. W. (2004). *J. Biol. Inorg. Chem.* **9**, 429–438.

Zang, T. M., Hollman, D. A., Crawford, P. A., Crowder, M. W. & Makaroff, C. A. (2001). *J. Biol. Chem.* **276**, 4788–4795.